We are IntechOpen, the world's leading publisher of Open Access books Built by scientists, for scientists

4,800
Open access books available

122,000
International authors and editors

135M
Downloads

Our authors are among the

154
Countries delivered to

TOP 1%
most cited scientists

12.2%
Contributors from top 500 universities

WEB OF SCIENCE™

Selection of our books indexed in the Book Citation Index in Web of Science™ Core Collection (BKCI)

Interested in publishing with us?
Contact book.department@intechopen.com

Numbers displayed above are based on latest data collected.
For more information visit www.intechopen.com

11

Inverse Scattering in the Low-Frequency Region by Using Acoustic Point Sources

Nikolaos L. Tsitsas
Department of Mathematics, School of Applied Mathematical and Physical Sciences, National Technical University of Athens, Athens Greece

1. Introduction

The interaction of a point-source spherical acoustic wave with a bounded obstacle possesses various attractive and useful properties in direct and inverse scattering theory. More precisely, concerning the direct scattering problem, the far-field interaction of a point source with an obstacle is, under certain conditions, stronger compared to that of a plane wave. On the other hand, in inverse scattering problems the distance of the point-source from the obstacle constitutes a crucial parameter, which is encoded in the far-field pattern and is utilized appropriately for the localization and reconstruction of the obstacle's physical and geometrical characteristics.

The research of point-source scattering initiated in (1), dealing with analytical investigations of the scattering problem by a circular disc. The main results for point-source scattering by simple homogeneous canonical shapes are collected in the classic books (2) and (3). The techniques of the low-frequency theory (4) in the point-source acoustic scattering by soft, hard, impedance surface, and penetrable obstacles were introduced in (5), (6), and (7), where also explicit results for the corresponding particular spherical homogeneous scatterers were obtained. Moreover, in (5), (6), and (7) simple far-field inverse scattering algorithms were developed for the determination of the sphere's center as well as of its radius. On the other hand, point-source near-field inverse scattering problems for a small soft or hard sphere were studied in (8). For other implementations of near-field inverse problems see (9), and p. 133 of (10); also we point out the point-source inverse scattering methods analyzed in (11).

In all the above investigations the incident wave is generated by a point-source located in the exterior of the scatterer. However, a variety of applications suggests the investigation of excitation problems, where a layered obstacle is excited by an acoustic spherical wave generated by a point source located in its interior. Representative applications concern scattering problems for the localization of an object, buried in a layered medium (e.g. inside the earth), (12). This is due to the fact that the Green's function of the layered medium (corresponding to an interior point-source) is utilized as kernel of efficient integral equation formulations, where the integration domain is usually the support of an inhomogeneity existing inside the layered medium. Besides, the interior point-source excitation of a layered sphere has significant medical applications, such as implantations inside the human head for hyperthermia or biotelemetry purposes (13), as well as excitation of the human brain by the neurons currents (see for example (14) and (15), as well as the references therein). Several

physical applications of layered media point-source excitation in seismic wave propagation, underwater acoustics, and biology are reported in (16) and (17). Further chemical, biological and physical applications motivating the investigations of interior and exterior scattering problems by layered spheres are discussed in (18). Additionally, we note that, concerning the experimental realization and configuration testing for the related applications, a point-source field is more easily realizable inside the limited space of a laboratory compared to a plane wave field.

To the direction of modeling the above mentioned applications, direct and inverse acoustic scattering and radiation problems for point source excitation of a piecewise homogeneous sphere were treated in (19).

This chapter is organized as follows: Section 2 contains the mathematical formulation of the excitation problem of a layered scatterer by an interior point-source; the boundary interfaces of the adjacent layers are considered to be $\mathcal{C}^2$ surfaces. The following Sections focus on the case where the boundary surfaces are spherical and deal with the direct and inverse acoustic point-source scattering by a piecewise homogeneous (layered) sphere. The point-source may be located either in the exterior or in the interior of the sphere. The layered sphere consists of N concentric spherical layers with constant material parameters; $N-1$ layers are penetrable and the N-th layer (core) is soft, hard, resistive or penetrable. More precisely, Section 3.1 addresses the direct scattering problem for which an analytic method is developed for the determination of the exact acoustic Green's function. In particular, the Green's function is determined analytically by solving the corresponding boundary value problem, by applying a combination of Sommerfeld's (20), (21) and T-matrix (22) methods. Also, we give numerical results on comparative far-field investigations of spherical and plane wave scattering, which provide quantitative criteria on how far the point-source should be placed from the sphere in order to obtain the same results with plane wave incidence. Next, in Section 3.2 the low-frequency assumption is introduced and the related far-field patterns and scattering cross-sections are derived. In particular, we compute the low-frequency approximations of the far-field quantities with an accuracy of order $\mathcal{O}((k_0 a_1)^4)$ (k_0 the free space wavenumber and a_1 the exterior sphere's radius). The spherical wave low-frequency far-field results reduce to the corresponding ones due to plane wave incidence on a layered sphere and also recover as special cases several classic results of the literature (contained e.g. in (2), and (5)-(7)), concerning the exterior spherical wave excitation of homogeneous small spheres, subject to various boundary conditions. Also, we present numerical simulations concerning the convergence of the low-frequency cross-sections to the exact ones. Moreover, in Section 3.3 certain low-frequency near-field results are briefly reported.

Importantly, in Section 4 various far- and near-field inverse scattering algorithms for a small layered sphere are presented. The main idea in the development of these algorithms is that the distance of the point source from the scatterer is an additional parameter, encoded in the cross-section, which plays a primary role for the localization and reconstruction of the sphere's characteristics. First, in Section 4.1 the following three types of far-field inverse problems are examined: (i) establish an algorithmic criterion for the determination of the point-source's location for given geometrical and physical parameters of the sphere by exploiting the different cross-section characteristics of interior and exterior excitation, (ii) determine the mass densities of the sphere's layers for given geometrical characteristics by combining the cross-section measurements for both interior and exterior point-source excitation, (iii) recover the sphere's location and the layers radii by measuring the total or differential cross-section for various exterior point-source locations as well as for plane wave incidence. Furthermore,

in Section 4.2 ideas on the potential use of point-source fields in the development of near-field inverse scattering algorithms for small layered spheres are pointed out.

2. Interior acoustic excitation of a layered scatterer: mathematical formulation

The *layered scatterer* V is a bounded and closed subset of $\mathbb{R}^3$ with $\mathcal{C}^2$ boundary S_1 possessing the following properties (see Fig. 1): (i) the interior of V is divided by $N-1$ surfaces S_j (j=2,...,N) into N annuli-like regions (layers) V_j (j=1,...,N), (ii) S_j are $\mathcal{C}^2$ surfaces with S_j containing S_{j+1} and $\text{dist}(S_j, S_{j+1}) > 0$, (iii) the layers V_j (j=1,...,$N-1$), are homogeneous isotropic media specified by real wavenumbers k_j and mass densities ρ_j, (iv) the scatterer's core V_N (containing the origin of coordinates) is penetrable specified by real wavenumber k_N and mass density ρ_N or impenetrable being soft, hard or resistive. The exterior V_0 of the scatterer V is a homogeneous isotropic medium with real constants k_0 and ρ_0. In any layer V_j the Green's second theorem is valid by considering the surfaces S_j as oriented by the outward normal unit vector $\hat{\mathbf{n}}$.

The layered scatterer V is excited by a time harmonic ($\exp(-i\omega t)$ time dependence) spherical acoustic wave, generated by a point source with position vector $\mathbf{r}_q$ in the layer V_q (q=0,...,N). Applying Sommerfeld's method (see for example (20), (21), (22)), the primary spherical field $u^{pr}_{\mathbf{r}_q}$, radiated by this point-source, is expressed by

$$u^{pr}_{\mathbf{r}_q}(\mathbf{r}) = r_q \exp(-ik_q r_q)\frac{\exp(ik_q|\mathbf{r}-\mathbf{r}_q|)}{|\mathbf{r}-\mathbf{r}_q|}, \qquad \mathbf{r}\in\mathbb{R}^3\backslash\{\mathbf{r}_q\}, \tag{1}$$

where r_q=$|\mathbf{r}_q|$. We have followed the normalization introduced in (5), namely considered that the primary field reduces to a plane wave with direction of propagation that of the unit vector $-\hat{\mathbf{r}}_q$, when the point source recedes to infinity, i.e.

$$\lim_{r_q\to\infty} u^{pr}_{\mathbf{r}_q}(\mathbf{r}) = \exp(-ik_q\hat{\mathbf{r}}_q\cdot\mathbf{r}). \tag{2}$$

The scatterer V perturbs the primary field $u^{pr}_{\mathbf{r}_q}$, generating *secondary fields* in every layer V_j. The respective secondary fields in V_j ($j\neq q$) and V_q are denoted by $u^{j}_{\mathbf{r}_q}$ and $u^{sec}_{\mathbf{r}_q}$. By Sommerfeld's method, the total field $u^{q}_{\mathbf{r}_q}$ in V_q is defined as the superposition of the primary and the secondary field

$$u^{q}_{\mathbf{r}_q}(\mathbf{r}) = u^{pr}_{\mathbf{r}_q}(\mathbf{r}) + u^{sec}_{\mathbf{r}_q}(\mathbf{r}), \quad \mathbf{r}\in V_q\setminus\{\mathbf{r}_q\}. \tag{3}$$

Moreover, the total field in V_j ($j\neq q$) coincides with the secondary field $u^{j}_{\mathbf{r}_q}$.

The total field $u^{j}_{\mathbf{r}_q}$ in layer V_j satisfies the Helmholtz equation

$$\Delta u^{j}_{\mathbf{r}_q}(\mathbf{r}) + k_j^2 u^{j}_{\mathbf{r}_q}(\mathbf{r}) = 0, \tag{4}$$

for $\mathbf{r}\in V_j$ if $j\neq q$ and $\mathbf{r}\in V_q\backslash\{\mathbf{r}_q\}$ if $j=q$.

On the surfaces S_q and S_{q+1} the following transmission boundary conditions are required

$$u^{q-1}_{\mathbf{r}_q}(\mathbf{r}) - u^{sec}_{\mathbf{r}_q}(\mathbf{r}) = u^{pr}_{\mathbf{r}_q}(\mathbf{r}), \qquad \mathbf{r}\in S_q$$

$$\frac{1}{\rho_{q-1}}\frac{\partial u^{q-1}_{\mathbf{r}_q}(\mathbf{r})}{\partial n} - \frac{1}{\rho_q}\frac{\partial u^{sec}_{\mathbf{r}_q}(\mathbf{r})}{\partial n} = \frac{1}{\rho_q}\frac{\partial u^{pr}_{\mathbf{r}_q}(\mathbf{r})}{\partial n}, \quad \mathbf{r}\in S_q \tag{5}$$

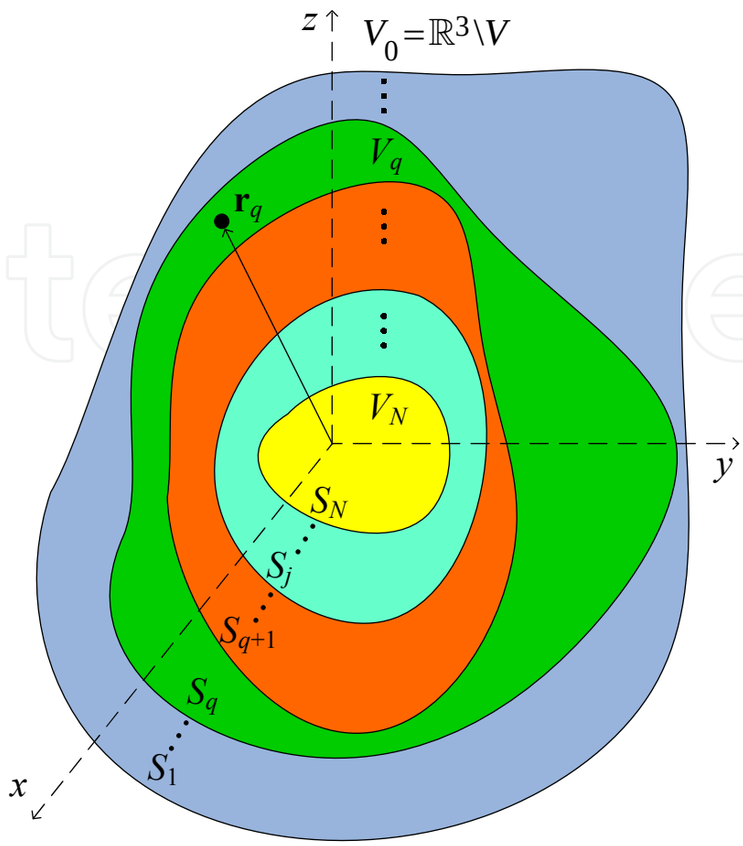

Fig. 1. Typical cross-section of the layered scatterer V.

$$u^{q+1}_{\mathbf{r}_q}(\mathbf{r}) - u^{sec}_{\mathbf{r}_q}(\mathbf{r}) = u^{pr}_{\mathbf{r}_q}(\mathbf{r}), \qquad \mathbf{r} \in S_{q+1}$$

$$\frac{1}{\rho_{q+1}} \frac{\partial u^{q+1}_{\mathbf{r}_q}(\mathbf{r})}{\partial n} - \frac{1}{\rho_q} \frac{\partial u^{sec}_{\mathbf{r}_q}(\mathbf{r})}{\partial n} = \frac{1}{\rho_q} \frac{\partial u^{pr}_{\mathbf{r}_q}(\mathbf{r})}{\partial n}, \quad \mathbf{r} \in S_{q+1} \tag{6}$$

Furthermore, on the surfaces S_j $(j \neq q, q+1, N)$ the total fields must satisfy the transmission conditions

$$u^{j-1}_{\mathbf{r}_q}(\mathbf{r}) - u^{j}_{\mathbf{r}_q}(\mathbf{r}) = 0, \quad \mathbf{r} \in S_j$$

$$\frac{1}{\rho_{j-1}} \frac{\partial u^{j-1}_{\mathbf{r}_q}(\mathbf{r})}{\partial n} - \frac{1}{\rho_j} \frac{\partial u^{j}_{\mathbf{r}_q}(\mathbf{r})}{\partial n} = 0, \quad \mathbf{r} \in S_j \tag{7}$$

For a penetrable core (7) hold also for j=N. On the other hand, for a soft, hard and resistive core the total field on S_N must satisfy respectively
the Dirichlet

$$u^{N-1}_{\mathbf{r}_q}(\mathbf{r}) = 0, \quad \mathbf{r} \in S_N \tag{8}$$

the Neumann

$$\frac{\partial u_{\mathbf{r}_q}^{N-1}(\mathbf{r})}{\partial n} = 0, \quad \mathbf{r} \in S_N \tag{9}$$

and the Robin boundary condition

$$\frac{\partial u_{\mathbf{r}_q}^{N-1}(\mathbf{r})}{\partial n} + ik_{N-1}\lambda u_{\mathbf{r}_q}^{N-1}(\mathbf{r}) = 0, \quad \mathbf{r} \in S_N \quad (\lambda \in \mathbb{R}). \tag{10}$$

The first of Eqs. (5), (6), (7) and Eq. (8) represent the continuity of the fluid's pressure, while the second of Eqs. (5), (6), (7) and Eq. (9) represent the continuity of the normal components of the wave's speed. Detailed discussion on the physical parameters of acoustic wave scattering problems is contained in (4).

Since scattering problems always involve an unbounded domain, a radiation condition for the total field in V_0 must be imposed. Thus, $u_{\mathbf{r}_q}^0$ must satisfy the Sommerfeld radiation condition (10)

$$\frac{\partial u_{\mathbf{r}_q}^0(\mathbf{r})}{\partial n} - ik_0 u_{\mathbf{r}_q}^0(\mathbf{r}) = o(r^{-1}), \quad r \to \infty \tag{11}$$

uniformly for all directions $\hat{\mathbf{r}}$ of $\mathbb{R}^3$, i.e. $\hat{\mathbf{r}} \in S^2 = \{\mathbf{x} \in \mathbb{R}^3, |\mathbf{x}| = 1\}$. Note that a primary spherical acoustic wave defined by (1) satisfies the Sommerfeld radiation condition (11), which clearly is not satisfied by an incident plane acoustic wave.

Besides, the secondary $u_{\mathbf{r}_0}^{sec}$ and the total field $u_{\mathbf{r}_q}^0$ in V_0 have the asymptotic expressions

$$u_{\mathbf{r}_0}^{sec}(\mathbf{r}) = g_{\mathbf{r}_0}(\hat{\mathbf{r}})h_0(k_0 r) + \mathcal{O}(r^{-2}), \quad r \to \infty \tag{12}$$

$$u_{\mathbf{r}_q}^0(\mathbf{r}) = g_{\mathbf{r}_q}(\hat{\mathbf{r}})h_0(k_0 r) + \mathcal{O}(r^{-2}), \quad r \to \infty \quad (q > 0) \tag{13}$$

where $h_0(x)$=exp$(ix)/(ix)$ is the zero-th order spherical Hankel function of the first kind. The function $g_{\mathbf{r}_q}$ is the *q-excitation far-field pattern* and describes the response of the scatterer in the direction of observation $\hat{\mathbf{r}}$ of the far-field, due to the excitation by the particular primary field $u_{\mathbf{r}_q}^{pr}$ in layer V_q.

Moreover, we define the *q-excitation differential* (or *bistatic radar*) *cross-section*

$$\sigma_{\mathbf{r}_q}(\hat{\mathbf{r}}) = \frac{4\pi}{k_0^2}|g_{\mathbf{r}_q}(\hat{\mathbf{r}})|^2, \tag{14}$$

which specifies the amount of the field's power radiated in the direction $\hat{\mathbf{r}}$ of the far field. Also, we define the *q-excitation total cross-section*

$$\sigma_{\mathbf{r}_q} = \frac{1}{k_0^2}\int_{S^2} |g_{\mathbf{r}_q}(\hat{\mathbf{r}})|^2 ds(\hat{\mathbf{r}}), \tag{15}$$

representing the average of the amount of the field's power radiated in the far-field over all directions, due to the excitation of the layered scatterer V by a point-source located in layer V_q. Thus, $\sigma_{\mathbf{r}_q}$ is the average of $\sigma_{\mathbf{r}_q}(\hat{\mathbf{r}})$ over all directions. We note that the definition (15) of $\sigma_{\mathbf{r}_q}$ extends that of the scattering cross-section (see (5) of (8) or (17) of (5)) due to a point-source at $\mathbf{r}_0 \in \mathbb{R}^3 \backslash V$.

Finally, we define the *absorption* and the *extinction cross-section*

$$\sigma_{\mathbf{r}_q}^{\mathrm{a}} = \frac{\rho_0}{\rho_{N-1}k_0}\mathrm{Im}\left[\int_{S_N} u_{\mathbf{r}_q}^{N-1}(\mathbf{r})\overline{\frac{\partial u_{\mathbf{r}_q}^{N-1}(\mathbf{r})}{\partial n}} ds(\mathbf{r})\right], \tag{16}$$

$$\sigma^{\mathrm{e}}_{\mathbf{r}_q} = \sigma^{\mathrm{a}}_{\mathbf{r}_q} + \sigma_{\mathbf{r}_q}. \tag{17}$$

The former determines the amount of primary field power, absorbed by the core V_N (since all the other layers have been assumed lossless) and the latter the total power that the scatterer extracts from the primary field either by radiation in V_0 or by absorption. Clearly, $\sigma^{\mathrm{a}}_{\mathbf{r}_q} = 0$ for a soft, hard, or penetrable lossless core, and $\sigma^{\mathrm{a}}_{\mathbf{r}_q} \geq 0$ for a resistive core.

We note that scattering theorems for the interior acoustic excitation of a layered obstacle, subject to various boundary conditions, have been treated in (23) and (24).

3. Layered sphere: direct scattering problems

The solution of the direct scattering problem for the layered scatterer of Fig. 1 cannot be obtained analytically and thus generally requires the use of numerical methods; for an overview of such methods treating inhomogeneous and partially homogeneous scatterers see (25). However, for spherical surfaces S_j, the boundary value problem can be solved analytically and the exact Green's function can be obtained in the form of special functions series. To this end, we focus hereafter to the case of the scatterer V being a *layered sphere*. By adjusting the general description of Section 2, the spherical scatterer V has radius a_1 and surface S_1, while the interior of V is divided by $N-1$ concentric spherical surfaces S_j, defined by $r = a_j$ (j=2,...,N) into N layers V_j (j=1,...,N) (see Fig. 2). The layers V_j, defined by $a_{j+1} \leq r \leq a_j$ (j=1,...,$N-1$), are filled with homogeneous materials specified by real wavenumbers k_j and mass densities ρ_j.

3.1 Exact acoustic Green's function

A classic scattering problem deals with the effects that a discontinuity of the medium of propagation has upon a known incident wave and that takes care of the case where the excitation is located outside the scatterer. When the source of illumination is located inside the scatterer and we are looking at the field outside it, then we have a radiation and not a scattering problem. The investigation of spherical wave scattering problems by layered spherical scatterers is usually based on the implementation of T-matrix (22) combined with Sommerfeld's methods (20), (21). The T-matrix method handles the effect of the sphere's layers and the Sommerfeld's method handles the singularity of the point-source and unifies the cases of interior and exterior excitation. The combination of these two methods leads to certain algorithms for the development of exact expressions for the fields in every layer. Here, we impose an appropriate combined Sommerfeld T-matrix method for the computation of the exact acoustic Green's function of a layered sphere. More precisely, the primary and secondary acoustic fields in every layer are expressed with respect to the basis of the spherical wave functions. The unknown coefficients in the secondary fields expansions are determined analytically by applying a T-matrix method.

We select the spherical coordinate system (r,θ,ϕ) with the origin O at the centre of V, so that the point-source is at r=r_q, θ=0. The primary spherical field (1) is then expressed as (19)

$$u^{pr}_{\mathbf{r}_q}(r,\theta) = \frac{1}{h_0(k_q r_q)} \begin{cases} \sum_{n=0}^{\infty}(2n+1) j_n(k_q r_q) h_n(k_q r) P_n(\cos\theta), & r > r_q \\ \sum_{n=0}^{\infty}(2n+1) h_n(k_q r_q) j_n(k_q r) P_n(\cos\theta), & r < r_q \end{cases}$$

where j_n and h_n are the n-th order spherical Bessel and Hankel function of the first kind and P_n is a Legendre polynomial.

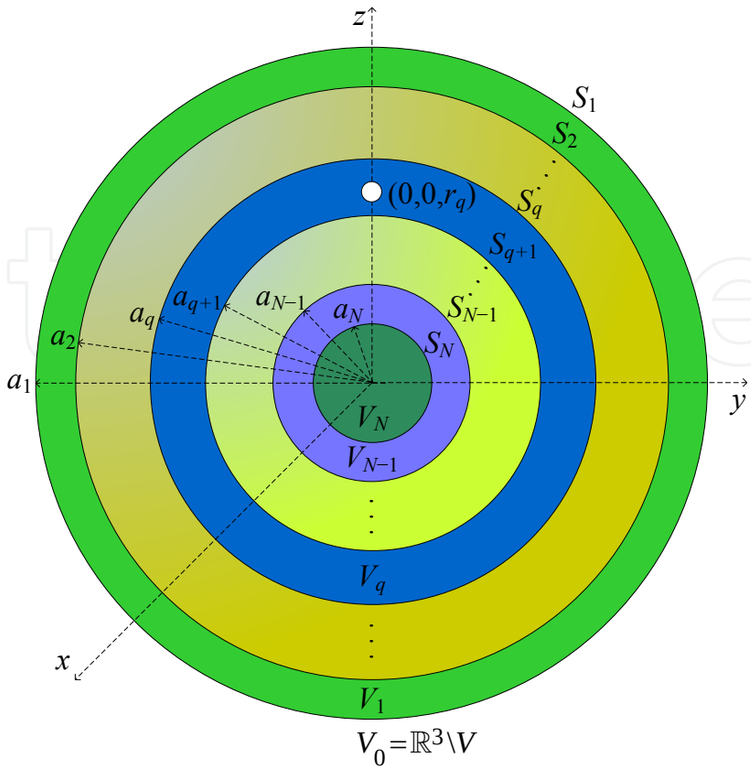

Fig. 2. Geometry of the layered spherical scatterer.

The secondary field $u^j_{\mathbf{r}_q}$ in V_j (j=1,...,$N-1$) is expanded as

$$u^j_{\mathbf{r}_q}(r,\theta) = \sum_{n=0}^{\infty}(2n+1)\frac{h_n(k_q r_q)}{h_0(k_q r_q)}\left(\alpha^j_{q,n} j_n(k_j r) + \beta^j_{q,n} h_n(k_j r)\right) P_n(\cos\theta), \tag{18}$$

where $\alpha^j_{q,n}$ and $\beta^j_{q,n}$ under determination coefficients. The secondary field in V_0 has the expansion (18) with j=0 and $\alpha^0_{q,n} = 0$, valid for $r \geq a_1$, in order that the radiation condition (11) is satisfied. On the other hand, since zero belongs to V_N, the secondary field in a penetrable core V_N has the expansion (18) with j=N and $\beta^N_{q,n}$=0, valid for $0 \leq r \leq a_N$.
By imposing the boundary conditions (7) on the spherical surfaces S_j, we obtain the transformations

$$\begin{bmatrix} \alpha^j_{q,n} \\ \beta^j_{q,n} \end{bmatrix} = \mathbf{T}^j_n \begin{bmatrix} \alpha^{j-1}_{q,n} \\ \beta^{j-1}_{q,n} \end{bmatrix} \tag{19}$$

The 2×2 transition matrix $\mathbf{T}^j_n$ from V_{j-1} to V_j, which is independent of the point-source's location, is given by

$$\mathbf{T}^j_n = -ix_j^2 \begin{bmatrix} h_n'(x_j)j_n(y_j) - w_j h_n(x_j)j_n'(y_j) & h_n'(x_j)h_n(y_j) - w_j h_n(x_j)h_n'(y_j) \\ w_j j_n(x_j)j_n'(y_j) - j_n'(x_j)j_n(y_j) & w_j j_n(x_j)h_n'(y_j) - j_n'(x_j)h_n(y_j) \end{bmatrix},$$

where $x_j = k_j a_j$, $y_j = k_{j-1} a_j$, $w_j = (k_{j-1}\rho_j)/(k_j \rho_{j-1})$.

Since $\alpha_{q,n}^{0}$=0, successive application of (19) for j=1,...,q leads to

$$\begin{bmatrix} \alpha_{q,n}^{q} \\ \beta_{q,n}^{q} + \frac{j_n(k_q r_q)}{h_n(k_q r_q)} \end{bmatrix} = \mathbf{T}_{q,n}^{+} \begin{bmatrix} 0 \\ \beta_{q,n}^{0} \end{bmatrix} \tag{20}$$

where

$$\mathbf{T}_{q,n}^{+} = \mathbf{T}_{n}^{q} ... \mathbf{T}_{n}^{2} \mathbf{T}_{n}^{1} \quad . \tag{21}$$

In a similar way successive application of (19) for j=q+1,...,$N-1$ gives

$$\begin{bmatrix} \alpha_{q,n}^{N-1} \\ \beta_{q,n}^{N-1} \end{bmatrix} = \mathbf{T}_{q,n}^{-} \begin{bmatrix} \alpha_{q,n}^{q} + 1 \\ \beta_{q,n}^{q} \end{bmatrix} \tag{22}$$

where

$$\mathbf{T}_{q,n}^{-} = \mathbf{T}_{n}^{N-1} ... \mathbf{T}_{n}^{q+2} \mathbf{T}_{n}^{q+1} \quad . \tag{23}$$

The superscripts + in (20) and − in (22) indicate approach of the layer V_q, containing the point-source, from the layers above and below respectively.

Then, the coefficient of the secondary field in layer V_0 is determined by combining (20) and (22) and imposing the respective boundary condition on the surface of the core V_N, yielding

$$\begin{aligned} \beta_{q,n}^{0} = & \left\{ j_n(k_q r_q) \left[f_n(k_{N-1} a_N) \left(\mathbf{T}_{q,n}^{-} \right)_{12} + g_n(k_{N-1} a_N) \left(\mathbf{T}_{q,n}^{-} \right)_{22} \right] \right. \\ & \left. - h_n(k_q r_q) \left[f_n(k_{N-1} a_N) \left(\mathbf{T}_{q,n}^{-} \right)_{11} + g_n(k_{N-1} a_N) \left(\mathbf{T}_{q,n}^{-} \right)_{21} \right] \right\} \cdot \\ & \left\{ h_n(k_q r_q) \left[f_n(k_{N-1} a_N) \left(\mathbf{T}_{q,n}^{-} \mathbf{T}_{q,n}^{+} \right)_{12} + g_n(k_{N-1} a_N) \left(\mathbf{T}_{q,n}^{-} \mathbf{T}_{q,n}^{+} \right)_{22} \right] \right\}^{-1} \end{aligned} \tag{24}$$

where

$$\begin{aligned} f_n = j_n, \quad & j_n', \quad \text{and} \quad j_n' + i\lambda j_n \\ g_n = h_n, \quad & h_n', \quad \text{and} \quad h_n' + i\lambda h_n \end{aligned}$$

for a soft, hard and resistive core respectively, while for a penetrable core we obtain

$$\beta_{q,n}^{0} = \frac{j_n(k_q r_q) \left(\mathbf{T}_{n}^{N} \mathbf{T}_{q,n}^{-} \right)_{22} - h_n(k_q r_q) \left(\mathbf{T}_{n}^{N} \mathbf{T}_{q,n}^{-} \right)_{21}}{h_n(k_q r_q) \left(\mathbf{T}_{n}^{N} \mathbf{T}_{q,n}^{-} \mathbf{T}_{q,n}^{+} \right)_{22}} . \tag{25}$$

Moreover, by using the above explicit expression for $\beta_{q,n}^{0}$ we see that the coefficients $\alpha_{q,n}^{j}$ and $\beta_{q,n}^{j}$, describing the field in layer V_j (j=1,2,...,N), are determined by successive application of the transformations (19).

By using the above method we recover (for q=0 and N=1) classic results of the literature, concerning the scattered field for the exterior point-source excitation of a homogeneous sphere (see for example (10.5) and (10.70) of (2) for a soft and a hard sphere).

A basic advantage of the proposed method is that the coefficients $\beta_{q,n}^{0,N+1}$ of the secondary field in the exterior V_0 of an N+1-layered spherical scatterer with penetrable core may be obtained directly by means of the coefficients $\beta_{q,n}^{0,N}$ of the corresponding N-layered scatterer by means of an efficient recursive algorithm (19).

Furthermore, for any type of core the q-excitation far field pattern is given by

$$g_{\mathbf{r}_q}(\theta) = \frac{1}{h_0(k_q r_q)} \sum_{n=0}^{\infty} (2n+1)(-i)^n \beta_{q,n}^0 h_n(k_q r_q) P_n(\cos\theta). \tag{26}$$

This expression follows by (12), (13) and (18) for j=0 and by taking into account the asymptotic expression $h_n(z) \sim (-i)^n h_0(z)$, $z \to \infty$. By (14) and (26) we get the q-excitation bistatic radar cross-section

$$\sigma_{\mathbf{r}_q}(\theta) = 4\pi r_q^2 \frac{k_q^2}{k_0^2} \left| \sum_{n=0}^{\infty} (2n+1)(-i)^n \beta_{q,n}^0 h_n(k_q r_q) P_n(\cos\theta) \right|^2. \tag{27}$$

Now, by combining (15) with (26) and using the Legendre functions orthogonality properties ((27), (7.122) and (7.123)), we get the expression of the q-excitation total cross-section

$$\sigma_{\mathbf{r}_q} = 4\pi r_q^2 \frac{k_q^2}{k_0^2} \sum_{n=0}^{\infty} (2n+1) |\beta_{q,n}^0 h_n(k_q r_q)|^2. \tag{28}$$

Next, we will give some numerical results concerning the far-field interactions between the point-source and the layered sphere. In particular, we will make a comparative far-field investigation of spherical and plane wave scattering, which provides certain numerical criteria on how far the point-source should be placed from the sphere in order to obtain the same results with plane wave incidence. This knowledge is important for the implementation of the far-field inverse scattering algorithms described in Section 4.1 below.

Figs. 3a, 3b, and 3c depict the normalized 0-excitation total cross-section $\sigma_{\mathbf{r}_0}/2\pi a_1^2$ as a function of $k_0 a_1$ for a soft, hard, and penetrable sphere for three different point-source locations, as well as for plane wave incidence. The cross-sections for spherical wave scattering are computed by means of (28). On the other hand, by using (28) and taking into account that $h_n(k_0 r_0) \sim (-i)^n h_0(k_0 r_0)$, $r_0 \to \infty$, we obtain

$$\sigma = \frac{4\pi}{k_0^2} \sum_{n=0}^{\infty} (2n+1) |\beta_{0,n}^0|^2,$$

which is utilized for the cross-sections computations due to plane wave scattering.

The cross-section curves reduce to those due to plane wave incidence for large enough distances between the point-source and the scatterer. The critical location of the point-source where the results are almost the same with those of plane wave incidence depends on the type of boundary condition on the sphere's surface. In particular, for point-source locations with distances of more than 8, 5, and 8 radii a_1 from the center of a soft, hard, and penetrable sphere, the results are the same with the ones corresponding to plane wave incidence. We note that those cross-section curves of Figs. 3a and 3b referring to plane wave incidence on a soft and hard sphere coincide with those of Figs. 10.5 and 10.12 of (2).

The 0-excitation total cross-section $\sigma_{\mathbf{r}_0}$ increases as the point-source approaches the sphere ($r_0 \to a_1$) and hence the effect of the spherical wave on the sphere's far-field characteristics increases compared with that of the plane wave. Moreover, $\sigma_{\mathbf{r}_0}$ of a penetrable sphere as a function of $k_0 a_1$ is very oscillatory (see Fig. 3c). These oscillations are due to the penetrable material of the sphere and hence do not appear in the cases of soft or hard sphere. Besides, Fig. 3c indicates that $\sigma_{\mathbf{r}_0}$ of a penetrable sphere is oscillatory also as $k_0 a_1 \to \infty$, while for the other cases converges rapidly.

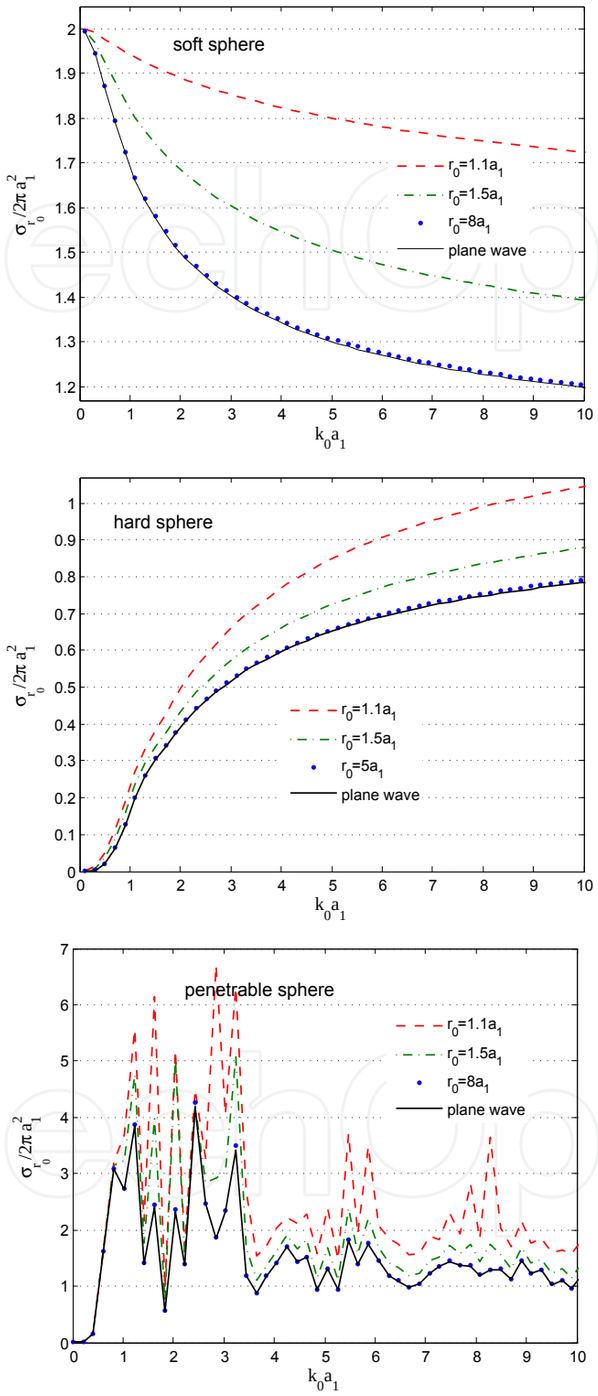

Fig. 3. Normalized 0-excitation total cross-section $\sigma_{\mathbf{r}_0}/2\pi a_1^2$ as a function of k_0a_1 for (a) a soft, (b) a hard, and (c) a penetrable (η_1=3, ϱ_1=2) sphere for various point-source locations and plane wave incidence

3.2 Far-field results for a small layered sphere

All formulae derived up to now are exact. Now, we make the so-called low-frequency assumption $k_0 a_1 \ll 1$ for the case of 3-layered sphere with any type of core, that is assume that the radius a_1 of the sphere is much smaller than the wavelength of the primary field. In order to establish the low-frequency results, we use the following dimensionless parameters

$$\xi_1 = a_1/a_2, \quad \xi_2 = a_2/a_3, \quad \varrho_i = \rho_i/\rho_0, \quad \eta_i = k_i/k_0, \quad \kappa = ik_0 a_1,$$

where ξ_1 and ξ_2 represent the thicknesses of layers V_1 and V_2 and ϱ_i and η_i the relative with respect to free space mass densities and refractive indices of layers V_i (i=1,2,3).
The following two cases are analyzed: (i) exterior excitation by a point-source located at (0,0,r_0) with $r_0 > a_1$, lying in the exterior V_0 of the sphere, and (ii) interior excitation by a point-source located at (0,0,r_1) with $a_2 < r_1 < a_1$, lying in layer V_1 of the 3-layered sphere. We define also

$$\tau_i = a_1/r_i, \qquad d = r_1/a_2 \qquad (i = 0, 1),$$

where τ_0 represents the distance of the exterior point-source from the sphere's surface and τ_1 and d the distances of the interior point-source from the boundaries of layer V_1.
Now, we distinguish the following cases according to the types of the core V_3.
(a) *V_3 is soft*
By using the asymptotic expressions of the spherical Bessel and Hankel functions for small arguments ((26), (10.1.4), (10.1.5)), from (24) we obtain

$$\beta_{q,0}^0 = \mathcal{S}_{q,0}^1 \kappa + \mathcal{S}_{q,0}^2 \kappa^2 + \mathcal{S}_{q,0}^3 \kappa^3 + \mathcal{O}(\kappa^4), \qquad \kappa \to 0 \qquad (q = 0, 1) \tag{29}$$

$$\beta_{0,n}^0 \sim \frac{(k_0 a_1)^{2n+1}}{i(2n+1)c_n^2} \mathcal{S}_{0,n}, \quad \beta_{1,n}^0 \sim \frac{\eta_1^n (k_0 a_1)^{2n+1}}{i c_n^2} \mathcal{S}_{1,n}, \qquad k_0 a_1 \to 0 \qquad (n \geq 1) \tag{30}$$

where

$$c_n = 1 \cdot 3 \cdot 5 \cdots (2n-1), \quad c_0 = 1,$$

and the quantities $\mathcal{S}_{q,0}^j$ (j=1,2,3) and $\mathcal{S}_{q,n}$ depend on the parameters ξ_1, ξ_2, ϱ_1, ϱ_2, d and are given in the Appendix of (19).
In order to calculate the q-excitation far-field patterns with an error of order κ^4, the coefficients $\beta_{q,0}^0$, $\beta_{q,1}^0$ and $\beta_{q,2}^0$ are sufficient. For $\kappa \to 0$, (26) gives the approximation of the q-excitation far-field patterns

$$g_{\mathbf{r}_0}(\theta) = \mathcal{S}_{0,0}^1 \kappa + \left[\mathcal{S}_{0,0}^2 + \tau_0 \mathcal{S}_{0,1} P_1(\cos\theta)\right] \kappa^2 + \left[\mathcal{S}_{0,0}^3 - \mathcal{S}_{0,1} P_1(\cos\theta) - \frac{\tau_0^2}{3} \mathcal{S}_{0,2} P_2(\cos\theta)\right] \kappa^3 + \mathcal{O}(\kappa^4) \tag{31}$$

$$g_{\mathbf{r}_1}(\theta) = \mathcal{S}_{1,0}^1 \kappa + \left[\mathcal{S}_{1,0}^2 + 3\tau_1 \mathcal{S}_{1,1} P_1(\cos\theta)\right] \kappa^2 + \left[\mathcal{S}_{1,0}^3 - 3\eta_1 \mathcal{S}_{1,1} P_1(\cos\theta) - \frac{5}{3} \tau_1^2 \mathcal{S}_{1,2} P_2(\cos\theta)\right] \kappa^3 + \mathcal{O}(\kappa^4) \tag{32}$$

By (28) the calculation of the q-excitation total cross-sections to the same accuracy requires only $\beta^0_{q,0}$ and $\beta^0_{q,1}$, giving for $\kappa \to 0$ the approximations

$$\sigma_{\mathbf{r}_0} = 4\pi a_1^2 \left\{ (\mathcal{S}^1_{0,0})^2 + k_0^2 a_1^2 \left[(\mathcal{S}^2_{0,0})^2 - 2\mathcal{S}^1_{0,0}\mathcal{S}^3_{0,0} + \frac{\tau_0^2}{3}(\mathcal{S}_{0,1})^2 \right] \right\} + \mathcal{O}(\kappa^4) \tag{33}$$

$$\sigma_{\mathbf{r}_1} = 4\pi a_1^2 \left\{ (\mathcal{S}^1_{1,0})^2 + k_0^2 a_1^2 \left[(\mathcal{S}^2_{1,0})^2 - 2\mathcal{S}^1_{1,0}\mathcal{S}^3_{1,0} + 3\tau_1^2(\mathcal{S}_{1,1})^2 \right] \right\} + \mathcal{O}(\kappa^4). \tag{34}$$

(b) *V_3 is hard*
The respective results are as follows

$$\beta^0_{q,0} = \mathcal{H}^1_{q,0}\kappa + \mathcal{H}^2_{q,0}\kappa^2 + \mathcal{H}^3_{q,0}\kappa^3 + \mathcal{O}(\kappa^5), \quad \kappa \to 0 \qquad (q = 0, 1) \tag{35}$$

$$\beta^0_{0,n} \sim \frac{n}{n+1}\frac{(k_0a_1)^{2n+1}}{i(2n+1)c_n^2}\mathcal{H}_{0,n}, \quad \beta^0_{1,n} \sim \frac{\eta_1^n(k_0a_1)^{2n+1}}{i(n+1)c_n^2}\mathcal{H}_{1,n}, \quad k_0a_1 \to 0 \quad (n \geq 1), \tag{36}$$

where the quantities $\mathcal{H}^j_{q,0}$ (j=1,2,3) and $\mathcal{H}_{q,n}$, depending on ξ_1, ξ_2, ϱ_1, ϱ_2, d, are given in the Appendix of (19).
Now, by using (26) and (28) we obtain the low-frequency expansions of the q-excitation far-field patterns and total cross-sections as $\kappa \to 0$

$$g_{\mathbf{r}_0}(\theta) = \frac{\tau_0}{2}\mathcal{H}_{0,1}P_1(\cos\theta)\kappa^2 + \left[\mathcal{H}^3_{0,0} - \frac{\mathcal{H}_{0,1}}{2}P_1(\cos\theta) - \frac{2\tau_0^2}{9}\mathcal{H}_{0,2}P_2(\cos\theta) \right]\kappa^3 + \mathcal{O}(\kappa^4), \tag{37}$$

$$g_{\mathbf{r}_1}(\theta) = \mathcal{H}^1_{1,0}\kappa + \left[\mathcal{H}^2_{1,0} + \frac{3}{2}\tau_1\mathcal{H}_{1,1}P_1(\cos\theta) \right]\kappa^2 + \left[\mathcal{H}^3_{1,0} - \frac{3}{2}\eta_1\mathcal{H}_{1,1}P_1(\cos\theta) + \frac{5}{9}\tau_1^2\mathcal{H}_{1,2}P_2(\cos\theta) \right]\kappa^3 + \mathcal{O}(\kappa^4), \tag{38}$$

$$\sigma_{\mathbf{r}_0} = \pi a_1^2 \frac{\tau_0^2}{3}(\mathcal{H}_{0,1})^2(k_0a_1)^2 + \mathcal{O}(\kappa^4) \tag{39}$$

$$\sigma_{\mathbf{r}_1} = 4\pi a_1^2 \left\{ (\mathcal{H}^1_{1,0})^2 + k_0^2 a_1^2 \left[(\mathcal{H}^2_{1,0})^2 - 2\mathcal{H}^1_{1,0}\mathcal{H}^3_{1,0} + \frac{3}{4}\tau_1^2(\mathcal{H}_{1,1})^2 \right] \right\} + \mathcal{O}(\kappa^4). \tag{40}$$

(c) *V_3 is penetrable*
From (25) we have

$$\beta^0_{1,0} = \mathcal{P}^1_{1,0}\kappa + \mathcal{P}^2_{1,0}\kappa^2 + \mathcal{P}^3_{1,0}\kappa^3 + \mathcal{O}(\kappa^4), \quad \kappa \to 0 \tag{41}$$

$$\beta^0_{0,n} \sim \frac{ink_0^{2n+1}a_1^{2n+1}}{c_n^2(2n+1)}\mathcal{P}_{0,n}, \quad \beta^0_{1,n} \sim \frac{i\eta_1^n(k_0a_1)^{2n+1}}{c_n^2}\mathcal{P}_{1,n} \quad k_0a_1 \to 0 \quad (n \geq 1), \tag{42}$$

where the quantities $\mathcal{P}^j_{1,0}$ (j=1,2,3) and $\mathcal{P}_{q,n}$ depend on the parameters ξ_1, ξ_2, ϱ_1, ϱ_2, ϱ_3, d and are given in the Appendix of (19).

From (26) we obtain for $\kappa \to 0$ the approximation of the q-excitation far-field patterns and total cross-sections

$$g_{\mathbf{r}_0}(\theta) = \kappa^2(\kappa - \tau_0)\mathcal{P}_{0,1}P_1(\cos\theta) + \frac{2}{3}\kappa^3\tau_0^2\mathcal{P}_{0,2}P_2(\cos\theta) + \mathcal{O}(\kappa^4), \tag{43}$$

$$g_{\mathbf{r}_1}(\theta) = \mathcal{P}_{1,0}^1\kappa + \left[\mathcal{P}_{1,0}^2 - 3\tau_1\mathcal{P}_{1,1}P_1(\cos\theta)\right]\kappa^2 + \left[\mathcal{P}_{1,0}^3 + 3\eta_1\mathcal{P}_{1,1}P_1(\cos\theta) + \frac{5}{3}\tau_1^2\mathcal{P}_{1,2}P_2(\cos\theta)\right]\kappa^3 + \mathcal{O}(\kappa^4), \tag{44}$$

$$\sigma_{\mathbf{r}_0} = -4\pi a_1^2\kappa^2\frac{\tau_0^2}{3}(\mathcal{P}_{0,1})^2 + \mathcal{O}(\kappa^4) \tag{45}$$

$$\sigma_{\mathbf{r}_1} = 4\pi a_1^2\left[(\mathcal{P}_{1,0}^1)^2 + k_0^2a_1^2\left((\mathcal{P}_{1,0}^2)^2 - 2\mathcal{P}_{1,0}^1\mathcal{P}_{1,0}^3 + 3\tau_1^2(\mathcal{P}_{1,1})^2\right)\right] + \mathcal{O}(\kappa^4). \tag{46}$$

For a small layered sphere with a resistive core the corresponding far-field results are given in (19).

We note that: (i) for a soft core the leading order terms of the far-field patterns $g_{\mathbf{r}_q}$ and total cross-sections $\sigma_{\mathbf{r}_q}$ are of order κ^1 and κ^0 independently of q, (ii) for a hard, resistive, and penetrable core the leading order terms of $g_{\mathbf{r}_q}$ and $\sigma_{\mathbf{r}_q}$ are of order κ^2 for q=0 and κ^1 and κ^0 for q=1. Thus, the interaction characteristics of spheres with hard, resistive, and penetrable cores change drastically for point-sources embedded inside the sphere. This last fact is exploited appropriately in certain inverse scattering algorithms, described below.

Now, concerning certain reductions of the above derived low-frequency far-field results, we note that the point-source incident field (1) for $r_0 \to \infty$ ($\tau_0 \to 0$) reduces to the plane wave (2). Thus, the preceding far-field results for $\tau_0 \to 0$ reduce to the respective ones, corresponding to the plane wave incidence on a 3-layered sphere with soft, hard, and penetrable core V_3 respectively. We remark that the leading term approximations of the 0-excitation cross-sections (39) and (45) for a hard and penetrable core are zero for $\tau_0 = 0$. Hence the interaction of a layered sphere with hard and penetrable core with an incident low-frequency field is weaker when the incident field is a plane wave than when it is a spherical wave.

Moreover, concerning the spherical wave excitation of a 2-layered sphere with various types of cores, the far-field results are derived by the respective above ones for $\xi_2 = 1$, $\varrho_2 = \varrho_1$, $\varrho_3 = \varrho_2$, and $\eta_2 = \eta_1$. On the other hand, the derived low-frequency far-field results recover (for $\xi_1 = \xi_2 = 1$, $\varrho_1 = \varrho_2 = 1$, $\eta_1 = \eta_2 = 1$) several results of the literature, concerning the exterior spherical wave excitation of 1-layered (homogeneous) small spheres, subject to various boundary conditions; for more details see (19). Besides, by letting also $\tau_0 \to 0$ they recover classic low-frequency far-field results for plane wave incidence; see (10.28) of (2) and (7.33), (7.35), (7.42), (7.53), (7.55) and (7.66) of (4).

Importantly, the convergence of the low-frequency total cross-section to the exact one plays a significant role in the inverse scattering algorithms described in Section 4 below. To this end, here we will investigate numerically the convergence of the low-frequency q-excitation total cross-section to the exact one for a 3-layered sphere with various types of cores. Figs. 4 and 5 depict the exact and low-frequency normalized q-excitation total cross-section $\sigma_{\mathbf{r}_q}/2\pi a_1^2$ as a function of k_0a_1 for a 3-layered sphere with soft and hard core. The exact total cross-sections are computed by means of (28), while the low-frequency ones by (33), (34), (39), and (40).

For small k_0a_1 the convergence of the low-frequency to the exact total cross-section is excellent for all types of cores with weak and strong coatings subject to both interior and exterior

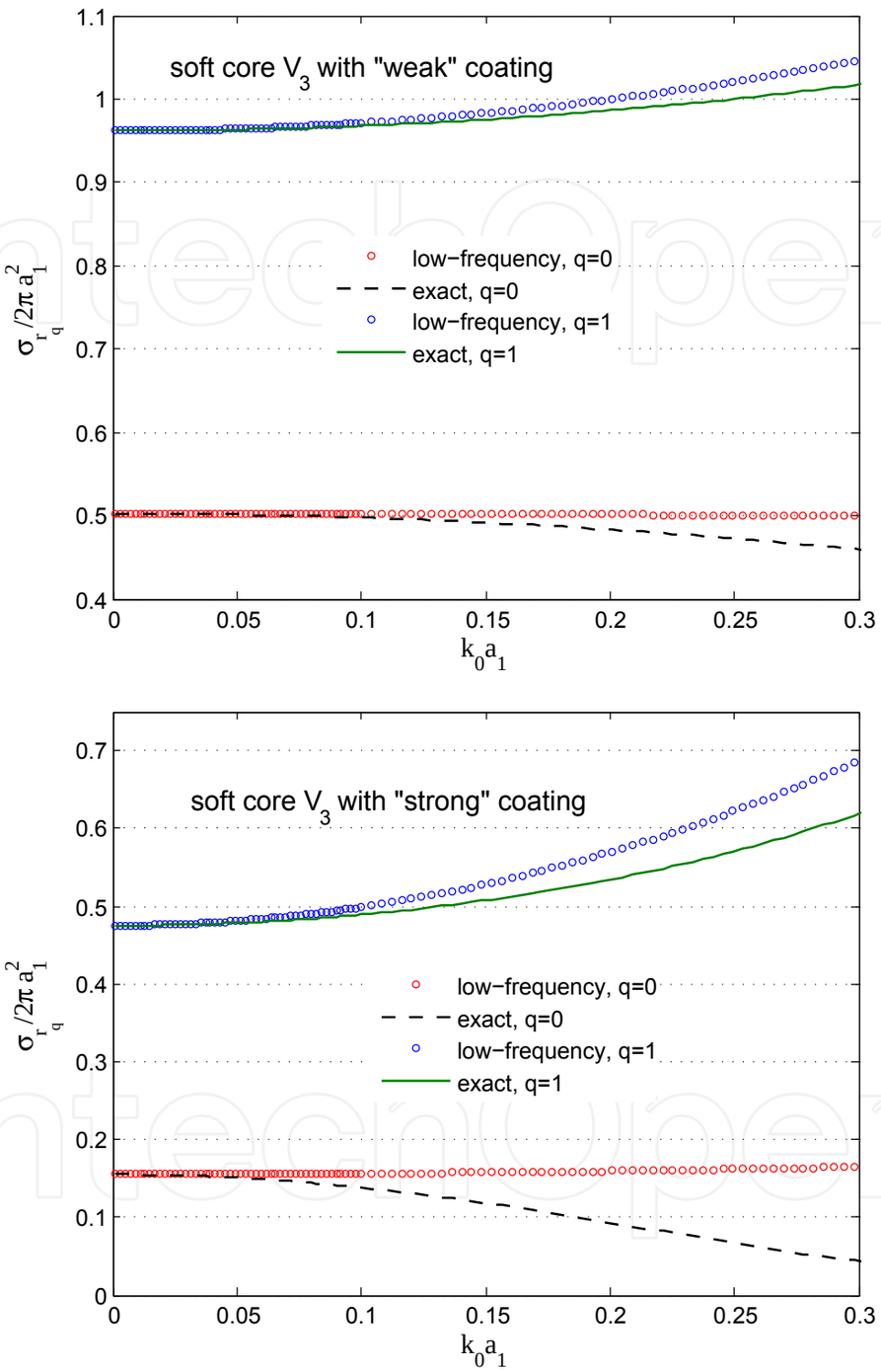

Fig. 4. Exact and low-frequency q-excitation total cross-section $\sigma_{\mathbf{r}_q}/2\pi a_1^2$ as a function of $k_0 a_1$ for a 3-layered sphere (a_2=0.5a_1, a_3=0.25a_1) with soft core with (a) weak (η_1=1.4, η_2=1.6, ϱ_1=1.2, ϱ_2=1.4), and (b) strong (η_1=2, η_2=3, ϱ_1=3, ϱ_2=2) coating. The two point-source locations are $r_0 = 1.1a_1$ and $r_1 = 1.1a_2$.

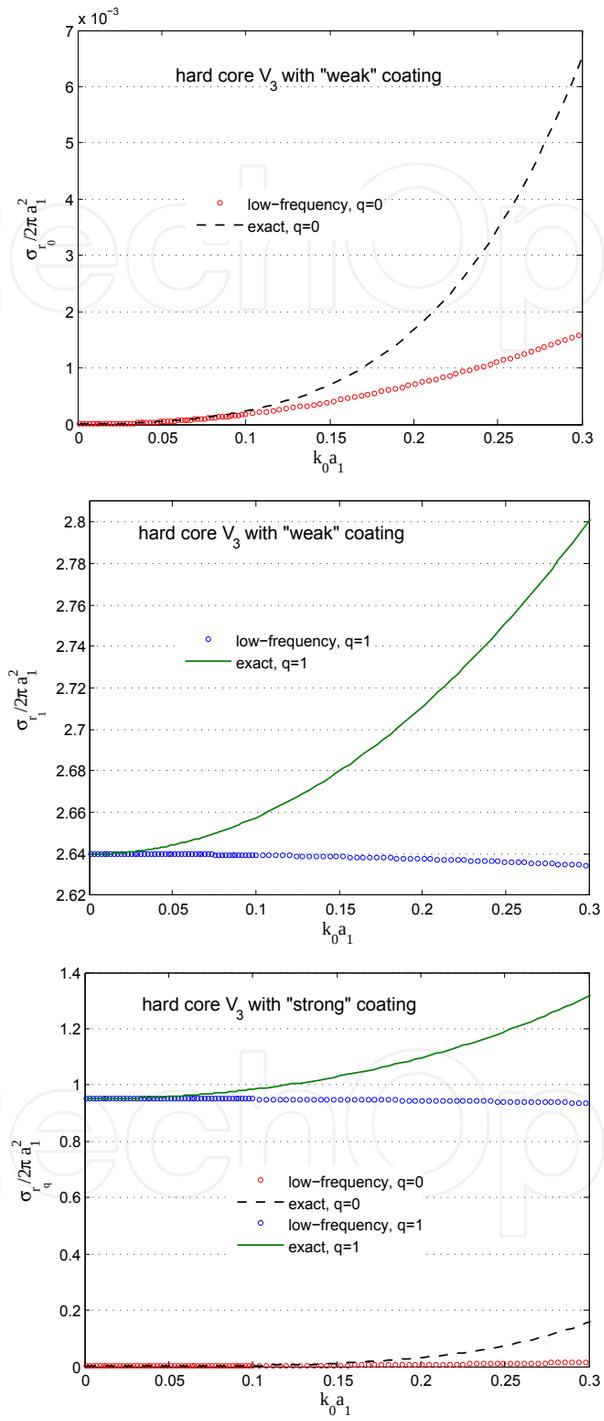

Fig. 5. Exact and low-frequency q-excitation total cross-section $\sigma_{\mathbf{r}_q}/2\pi a_1^2$ as a function of $k_0 a_1$ for a 3-layered sphere with hard core with (a) and (b) weak, and (c) strong coating.

excitation. However, even for $k_0 a_1$ lying outside the low-frequency region, good convergence is also achieved.
In the low-frequency region, the 1-excitation total cross-sections are much larger than the 0-excitation ones. This is the reverse situation to that occurring outside the low-frequency region, as discussed above, where the 0-excitation cross-section is larger that the 1-excitation. So, interior and exterior excitations constitute control mechanisms of the far-field intensity, depending on the desired application.

3.3 Near-field results for a small layered sphere

We consider a 2-layered sphere with soft core excited by an exterior source and still continue to adopt the low-frequency assumption $k_0 a_1 \ll 1$, that is we assume that the outer radius of the layered sphere, a_1, is much smaller than the wavelength of the primary field. More precisely, we suppose that $k_0 a_1$, $k_0 r_0$, $k_1 a_2$ and $k_1 r_q$ are all small (the waves are long compared to all geometrical lengths) whereas k_1/k_0 and ρ_1/ρ_0 are not assumed to be small. We define and use the following dimensionless parameters

$$\xi = a_1/a_2, \quad \varrho = \rho_1/\rho_0, \quad \eta = k_1/k_0, \quad \kappa = k_0 a_1, \quad \tau_0 = a_1/r_0, \quad d_1 = r_1/a_2 = \xi/\tau_1. \tag{47}$$

We use the asymptotic expressions of the spherical Bessel and Hankel functions for small arguments ((26), (10.1.4), (10.1.5)) to obtain the approximations of the elements of the transition matrix (19), as $\kappa \to 0$, by means of which we derive approximations for the field coefficients $\alpha_{0,n}^j$ and $\beta_{0,n}^j$. Then we estimate the secondary field at the source point, using

$$u_{\mathbf{r}_0}^{sec}(r_0, 0) = h_0(k_0 r_0) \sum_{n=0}^{\infty} (2n+1) \beta_{0,n}^0 [\mathscr{H}_n(k_0 r_0)]^2, \tag{48}$$

where

$$\mathscr{H}_n(w) = h_n(w)/h_0(w).$$

Moreover, from (30), we get

$$\beta_{0,n}^0 \sim \frac{\kappa^{2n+1}}{i(2n+1)c_n^2} \, \mathcal{S}_{0,n}(\xi, \varrho), \qquad \kappa \to 0, \tag{49}$$

where

$$\mathcal{S}_{0,n}(\xi, \varrho) = \frac{\mathcal{B}_n(\xi) + \varrho \, n \mathcal{A}_n(\xi)}{\Delta_n(\xi, \varrho)}, \quad \Delta_n(\xi, \varrho) = \mathcal{B}_n(\xi) - \varrho \, (n+1) \mathcal{A}_n(\xi), \tag{50}$$

$$\mathcal{A}_n(x) = 1 - x^{2n+1}, \quad \mathcal{B}_n(x) = n(x^{2n+1} + 1) + 1.$$

Now, since

$$\mathscr{H}_n(w) \sim c_n w^{-n} \qquad \text{as} \qquad w \to 0,$$

the small-κ approximation of (48) combined with (49) gives the following approximation of the secondary field at the external point-source's location

$$u_{\mathbf{r}_0}^{sec}(r_0, 0) = -\tau_0 \, \exp(ik_0 r_0) \sum_{n=0}^{\infty} \mathcal{S}_n(\xi, \varrho) \, \tau_0^{2n} + \mathcal{O}(\kappa), \tag{51}$$

as $k_0 a \to 0$. Note that, contrary to the case of low-frequency far-field results (see for example (19)), in the near-field every term of the infinite series contributes to the leading order $\mathcal{O}(1)$ behaviour. Now, by means of (51) we get

$$|u^{sec}_{\mathbf{r}_0}(r_0,0)| = \left| \tau_0 \sum_{n=0}^{\infty} \mathcal{S}_n(\xi,\varrho)\, \tau_0^{2n} \right| + \mathcal{O}(\kappa^2), \tag{52}$$

as $k_0 a \to 0$.

4. Layered sphere: inverse scattering problems

The low-frequency far- and near-field results, presented in Sections 3.2 and 3.3, are now utilized for the development of far- and near-field inverse scattering algorithms for the localization and reconstruction of the sphere's characteristics.

4.1 Far-field inverse scattering problems

The low-frequency realm offers a better environment for inverse scattering, compared to the exact yet complicated far-field series solutions (26) and (28), since the corresponding low-frequency far-field patterns are much more tractable. In particular, we develop inverse scattering algorithms for the determination of the geometrical and physical characteristics of the 3-layered sphere and the point-source, based on low-frequency measurements of the 0- and 1- excitation total cross-section. Additionally, we emphasize that the embedding of the point-source inside the scatterer offers additional essential information for the problem's characteristics, which cannot be given by a point-source outside the sphere.

4.1.1 Determination of the point-source's location

We determine the location of the point-source for given geometrical and physical characteristics of the sphere. This type of problem is expected to find applications in the determination of the layer that the neuron currents radiate in investigations of the human brain's activity (15). An inverse scattering algorithm is established for the hard core case.

We use the 0- and 1- excitation total cross-sections (39) and (40) of a 3-layered sphere with hard core. The decision on whether the point-source lies in the interior or the exterior of the sphere is based on the following *algorithmic criterion*:

Measure the leading term (of order $(k_0 a_1)^0$) in the low-frequency expansion of the total cross-section. If this measurement is zero, then from (39), the point-source is outside the sphere. On the other hand, if this measurement is not zero then from (40) the point-source is inside the sphere.

After determining the layer that the point-source is lying, we can also obtain its position r_q (q=0,1). For exterior excitation, we compute the position r_0 from the measurement of the leading order term of the 0-excitation total cross-section (39)

$$m_0 = \pi k_0^2 \frac{a_1^6}{3 r_0^2} (\mathcal{H}_{0,1})^2,$$

while for interior excitation, the measurement of the second order term of the 1-excitation total cross-section (40)

$$m_1 = 4\pi k_0^2 a_1^4 \left[(\mathcal{H}_{1,0}^2)^2 - 2\mathcal{H}_{1,0}^1 \mathcal{H}_{1,0}^3 + \frac{3a_1^2}{4r_1^2} (\mathcal{H}_{1,1})^2 \right]$$

gives the position r_1 of the point-source.

4.1.2 Determination of the layers material parameters

We determine the mass densities of the sphere's layers for given center's coordinates and layers radii of the sphere. Inverse scattering algorithms are established for a sphere with penetrable core.

Consider two point-source locations (0,0,b_0) and (0,0,b_1) with known distances $b_0 > a_1$ and $a_2 < b_1 < a_1$ from the layered sphere's center (that is the first point-source lies in the exterior and the second one in the interior of the scatterer). First, measure the leading order low-frequency term m_0 of the 0-excitation total cross-section (45) for a point-source at (0,0,b_0)

$$m_0 = \frac{4\pi k_0^2 a_1^6}{3b_0^2} (\mathcal{P}_{0,1})^2, \tag{53}$$

and then the leading m_1 and the second order term m_2 of the 1-excitation total cross-section (46) for a point-source at (0,0,b_1)

$$m_1 = 4\pi \frac{b_1^2}{\varrho_1^2}, \tag{54}$$

$$m_2 = 4\pi k_0^2 a_1^4 \left((\mathcal{P}_{1,0}^2)^2 - 2\mathcal{P}_{1,0}^1 \mathcal{P}_{1,0}^3 + \frac{3a_1^2}{b_1^2} (\mathcal{P}_{1,1})^2 \right). \tag{55}$$

Eq. (54) provides the mass density ϱ_1 of layer V_1. Eqs. (53) and (55) constitute a 2×2 non-linear system, the solution of which provides the densities ϱ_2 and ϱ_3 of layers V_2 and V_3.

4.1.3 Determination of the sphere's center and the layers radii

We determine the center's coordinates and the layers radii of the 3-layered sphere for given mass densities and refractive indices of the sphere's layers. We establish the inverse scattering algorithms for a sphere with soft core.

Choose a Cartesian coordinate system $Oxyz$ and five point-source locations (0,0,0), (ℓ,0,0), (0,ℓ,0), (0,0,ℓ), and (0,0,2ℓ) with unknown distances b_1, b_2, b_3, b_4 and b_5 from the layered sphere's center. The parameter ℓ represents a chosen fixed length. First, measure the leading order low-frequency term m_0 of the 0-excitation total cross-section (33) for a point-source located at the origin

$$m_0 = 4\pi a_1^2 (\mathcal{S}_{0,0}^1)^2 \tag{56}$$

Then, measure the second order low-frequency term m_j of the 0-excitation total cross-section (33) for each point-source location

$$m_j = 4\pi k_0^2 a_1^4 \left[(\mathcal{S}_{0,0}^2)^2 - 2\mathcal{S}_{0,0}^1 \mathcal{S}_{0,0}^3 + \frac{a_1^2}{3b_j^2} (\mathcal{S}_{0,1})^2 \right] \quad (j = 1, \ldots, 5)$$

Measurability techniques permitting the isolation of the individual measurements m_0 and m_j from the total cross-section measurements as well as measurement sensitivity aspects are discussed in (5).
Next, measure the second order cross-section term m_6 for a point-source far away from the sphere ($\tau \to 0$) (namely for plane wave incidence)

$$m_6 = 4\pi k_0^2 a_1^4 \left[(\mathcal{S}_{0,0}^2)^2 - 2\mathcal{S}_{0,0}^1 \mathcal{S}_{0,0}^3 \right] \tag{57}$$

We define the dimensionless quantities

$$\gamma_j = \frac{\ell}{\sqrt{m_j - m_6}} = \sqrt{\frac{3}{4\pi}} \frac{\ell}{k_0 a_1^2 \mathcal{S}_{0,1}} \frac{b_j}{a_1}. \tag{58}$$

Now, we have seven equations with the eight unknowns a_1, a_2, a_3, and b_j. The 8-th equation is derived by the law of cosines

$$b_5^2 = 2\ell^2 + 2b_4^2 - b_1^2, \tag{59}$$

and thus from (58) and (59) we get

$$\left(\frac{b_j}{\ell} \right)^2 = \frac{2\gamma_j^2}{\gamma_5^2 - 2\gamma_4^2 + \gamma_1^2},$$

which determine the distances b_j. The intersection point of the four spheres centered at (0,0,0), (ℓ,0,0), (0,ℓ,0), (0,0,ℓ) with determined radii b_1, b_2, b_3, b_4 coincides with the center of the layered spherical scatterer.
Finally, (56), (57), and (58) for j=1 constitute the 3×3 non-linear system

$$a_1 \mathcal{S}_{0,0}^1 = \sqrt{m_0/4\pi}$$

$$a_1^4 \left[(\mathcal{S}_{0,0}^2)^2 - 2\mathcal{S}_{0,0}^1 \mathcal{S}_{0,0}^3 \right] = m_6/(4\pi k_0^2)$$

$$a_1^3 \mathcal{S}_{0,1} = (\sqrt{3} b_1 \ell)/(\sqrt{4\pi} k_0 \gamma_1),$$

which gives as solutions the layers radii a_1, a_2, and a_3.

4.2 Near-field inverse scattering problems

The derived low-frequency near-field expansions in Section 3.3 are now utilized to establish inverse scattering algorithms for the determination of the geometrical characteristics of the piecewise homogeneous sphere. More precisely, the near-field inverse problem setting is as follows: we know the sphere's radius, a_1, as well as the location of its center and we are interested in estimating the core's radius, a_2. Note that for problems, where we need to determine also the sphere's radius and its center, appropriate modifications of the far-field algorithms (to the present context of near-field measurements) presented in Section 6.1 of (19) may be applied.

Consider a 2-layered sphere with soft core. We suppose that the radius a_1 and the density ϱ are known and we will estimate the core's radius a_2 by using a single measurement of the near-field due to an exterior point-source. The corresponding near-field at the exterior point-source's location is given by (52). The series appearing in (52), namely

$$\mathscr{S}(\xi,\tau_0,\varrho)=\sum_{n=0}^{\infty}\frac{\mathcal{B}_n(\xi)+\varrho\, n\mathcal{A}_n(\xi)}{\mathcal{B}_n(\xi)-\varrho\,(n+1)\mathcal{A}_n(\xi)}\tau_0^{2n}, \tag{60}$$

may be expressed with the aid of Gauss hypergeometric functions, if we consider that the relative mass density ϱ of the coating's layer V_1 is close to 1. For this case, the series (60) has the following properties

$$\mathscr{S}(\xi,\tau_0,1)=\frac{1}{\xi}\sum_{n=0}^{\infty}\frac{1}{2n+1}\left(\frac{\tau_0^2}{\xi^2}\right)^n=\frac{1}{2\tau_0}\ln\left(\frac{\xi+\tau_0}{\xi-\tau_0}\right), \tag{61}$$

$$\begin{aligned}\frac{\partial\mathscr{S}}{\partial\varrho}(\xi,\tau_0,1)&=\frac{1}{\xi^2}\sum_{n=0}^{\infty}\frac{n\xi^{2n+1}+n+1}{2n+1}(1-\xi^{2n+1})\left(\frac{\tau_0^2}{\xi^4}\right)^n\\&=\frac{1}{\xi^2}F\left(2;\frac{1}{2};\frac{3}{2};\frac{\tau_0^2}{\xi^4}\right)-\frac{\tau_0^2}{3}F\left(2;\frac{3}{2};\frac{5}{2};\tau_0^2\right)-\frac{1}{2\tau_0}\ln\left(\frac{\xi+\tau_0}{\xi-\tau_0}\right),\end{aligned} \tag{62}$$

where $F\equiv {}_2F_1$ is the Gauss hypergeometric function (26). Now, by considering the best linear approximation around the fixed point $\varrho=1$, from (60)-(62), we get

$$\begin{aligned}\mathscr{S}(\xi,\tau_0,\varrho)&\simeq\mathscr{S}(\xi,\tau_0,1)+\frac{\partial\mathscr{S}(\xi,\tau_0,1)}{\partial\varrho}(\varrho-1)\\&=\frac{1}{2\tau_0}\ln\left(\frac{\xi+\tau_0}{\xi-\tau_0}\right)(2-\varrho)-\left[\frac{1}{\xi^2}F\left(2;\frac{1}{2};\frac{3}{2};\frac{\tau_0^2}{\xi^4}\right)-\frac{\tau_0^2}{3}F\left(2;\frac{3}{2};\frac{5}{2};\tau_0^2\right)\right](1-\varrho),\end{aligned}$$

which in combination with (52) and (60) gives

$$\begin{aligned}|u^{sec}_{\mathbf{r}_0}(r_0,0)|=\Bigg|&\frac{2-\varrho}{2}\ln\left(\frac{\xi+\tau_0}{\xi-\tau_0}\right)\\&-\left[\frac{\tau_0}{\xi^2}F\left(2;\frac{1}{2};\frac{3}{2};\frac{\tau_0^2}{\xi^4}\right)-\frac{\tau_0^3}{3}F\left(2;\frac{3}{2};\frac{5}{2};\tau_0^2\right)\right](1-\varrho)\Bigg|+\mathcal{O}(\kappa^2).\end{aligned} \tag{63}$$

The radius a_2 of the core of the 2-layered sphere may now be determined by means of (63) as follows. We measure the leading order term in the above low-frequency expansion of $|u^{sec}_{\mathbf{r}_0}(r_0,0)|$, and we obtain a non-linear equation with respect $\xi=a_1/a_2$. Since, the radius a_1 is known, the solution of this equation provides the core's radius a_2.
Similar near-field algorithms may be developed for a 2-layered sphere with hard, and penetrable core.

5. Acknowledgement

The author's work was supported by the State Scholarships Foundation, while he was a post-doctoral research scholar.

6. References

[1] D. S. Jones, A new method for calculating scattering with particular reference to the circular disc, *Commun. Pure Appl. Math.* 9 (1956) 713–746.

[2] J. J. Bowman, T. B. Senior, P. L. Uslenghi, *Electromagnetic and Acoustic Scattering by Simple Shapes*, North Holland Publ. Co., 1969.

[3] D. S. Jones, *Acoustic and Electromagnetic Waves*, Oxford University Press, 1986.

[4] G. Dassios and R. Kleinman, *Low Frequency Scattering*, Clarendon Press, 2000.

[5] G. Dassios and G. Kamvyssas, Point source excitation in direct and inverse scattering: the soft and the hard small sphere, *IMA J. Appl. Math.* 55 (1995) 67–84.

[6] G. Dassios and G. Kamvyssas, The impedance scattering problem for a point-source field. The small resistive sphere, *Quart. J. Mech. Appl. Math.* 50 (1997) 321–332.

[7] G. Dassios, M. Hadjinicolaou and G. Kamvyssas, Direct and Inverse Scattering for Point Source Fields. The Penetrable Small Sphere, *Z. Angew. Math. Mech.* 79 (1999) 303–316.

[8] C. Athanasiadis, P.A. Martin and I.G. Stratis, On spherical-wave scattering by a spherical scatterer and related near-field inverse problems, *IMA J. Appl. Math.* 66 (2001) 539–549.

[9] C. J. S. Alves, and P. M. C. Ribeiro, Crack detection using spherical incident waves and near-field measurements. *Boundary Elements XXI*, edited by C. A. Brebbia and H. Power (WIT Press, Southampton, 1999) 355–364.

[10] D. Colton and R. Kress, *Inverse acoustic and electromagnetic scattering theory*, Springer-Verlag, 1992.

[11] R. Potthast, *Point-Sources and Multipoles in Inverse-Scattering Theory*, Chapman and Hall/CRC, 2001.

[12] J. Coyle, Locating the support of objects contained in a two-layered background medium in two dimensions, *Inverse Problems* 16 (2000) 275–292.

[13] J. Kim and Y. Rahmat-Samii, Implanted Antennas Inside a Human Body: Simulations, Designs, and Characterizations, *IEEE Trans. Microwave Theory Tech.* 52 (2004) 1934–1943.

[14] G. Dassios, A. S. Fokas and F. Kariotou, On the non-uniqueness of the inverse magnetoencephalography problem, *Inverse Problems* 21 (2005) L1–L5.

[15] G. Dassios, On the hidden electromagnetic activity of the brain, in: Mathematical Methods in Scattering Theory and Biomedical Engineering, Proceedings of the Seventh International Workshop, World Scientific Publishing Co., 2006, pp. 297–303.

[16] K. Aki and P. G. Richards, *Quantitative Seismology. Theory and Methods*, Freeman, 1980.

[17] A. E. Yagle and B. C. Levy, Application of the Schur algorithm to the inverse problem for a layered acoustic medium, *J. Acoust. Soc. Am.* 76 (1984) 301–308.

[18] A. Moroz, A recursive transfer-matrix solution for a dipole radiating inside and outside a stratified sphere, *Annals of Physics* 315, (2005) 352–418.

[19] N. L. Tsitsas, and C. Athanasiadis, Point source excitation of a layered sphere: direct and far-field inverse scattering problems, *Quart. J. Mech. Appl. Math.* 61, (2008) 549–580.

[20] A. Sommerfeld, *Partial Differential Equations in Physics*, Academic Press, 1949.

[21] J. A. Stratton, *Electromagnetic Theory*, McGraw-Hill, 1941.

[22] N. L. Tsitsas and C. Athanasiadis, On the scattering of spherical electromagnetic waves by a layered sphere, *Quart. J. Mech. Appl. Math.* 59 (2006) 55–74.

[23] C. Athanasiadis, N. L. Tsitsas, Scattering theorems for acoustic excitation of a layered obstacle by an interior point source, *Stud. Appl. Math.* 118 (2007), 397–418.

[24] N. L. Tsitsas, C. Athanasiadis, On the interior acoustic and electromagnetic excitation of a layered scatterer with a resistive or conductive core, *Bull. Greek Math. Soc.* 54 (2007) 127–141.
[25] W. C. Chew, *Waves and Fields in Inhomogeneous Media*, IEEE Press, New York, 1995.
[26] M. Abramowitz and I. A. Stegun. *Handbook of Mathematical Functions*, Dover, 1965.
[27] I. S. Gradshteyn and I. M. Ryzhik. *Table of Integrals, Series and Products*, Academic Press, 2000.

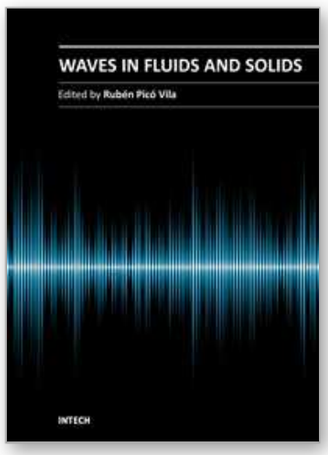

Waves in Fluids and Solids

Edited by Prof. Ruben Pico Vila

ISBN 978-953-307-285-2
Hard cover, 314 pages
Publisher InTech
Published online 22, September, 2011
Published in print edition September, 2011

Acoustics is an discipline that deals with many types of fields wave phenomena. Originally the field of Acoustics was consecrated to the sound, that is, the study of small pressure waves in air detected by the human ear. The scope of this field of physics has been extended to higher and lower frequencies and to higher intensity levels. Moreover, structural vibrations are also included in acoustics as a wave phenomena produced by elastic waves. This book is focused on acoustic waves in fluid media and elastic perturbations in heterogeneous media. Many different systems are analyzed in this book like layered media, solitons, piezoelectric substrates, crystalline systems, granular materials, interface waves, phononic crystals, acoustic levitation and soft media. Numerical methods are also presented as a fourth-order Runge-Kutta method and an inverse scattering method.

InTech Europe
University Campus STeP Ri
Slavka Krautzeka 83/A
51000 Rijeka, Croatia
Phone: +385 (51) 770 447
Fax: +385 (51) 686 166
www.intechopen.com

InTech China
Unit 405, Office Block, Hotel Equatorial Shanghai
No.65, Yan An Road (West), Shanghai, 200040, China
中国上海市延安西路65号上海国际贵都大饭店办公楼405单元
Phone: +86-21-62489820
Fax: +86-21-62489821

IntechOpen